Chapter 7 Effect of Sn Dopant on the Properties of ZnO Nanowires

7.0 Preface

The Sn doped ZnO (SZO) nanowires were fabricated by a vapor-liquid-solid (VLS) growth process. The reaction temperature for the formation of the nanowires can be reduced to ~100 ^{o}C due to Sn doping. The growth direction and morphology of SZO nanowires depend on the amount of Sn, which is attributed to different size between Zn and Sn atoms. The ultra-violet (UV) emission of SZO nanowires varies from 380 to 396 nm since Sn acts as a doubly ionized donor and introduces deep states in the band gap. In addition, the SZO nanowires exhibit significantly improved field emission characteristics with a turn-on electric field of 0.05 V/μm under a current density of 0.5 mA/cm^2 in comparison with undoped ZnO nanowires. The work function of the SZO nanowire decreases for the higher carrier concentration and the field enhancement factor increases for the smaller diameters. Also, the resistance of the SZO nanowire is decreased for the higher Sn mole fraction. Therefore, the SZO nanowires are excepted to be applicable to nano laser and flat panel display in the future.

7.1 Introduction

ZnO, a direct band gap (3.37eV) semiconductor with exciton binding energy of 60 meV, is a suitable material for optical application. The interesting

ZnO nano structures, such as nanowires[257], nanobelts[258], and nanoneedles[259] have drawn much attention in the understanding of their growth mechanism, physical properties, optical characteristics and field emission applications[260-264]. Recently, it has been reported that the larger aspect ratio of the ZnO nanowires used in field emission study can provide lower threshold power density[265-268]. The vapor-liquid-solid (VLS) process[269-271] has the advantages of high aspect ratio, geometric control, low production cost and large area deposition over other growth methods like metal-organic vapor phase epitaxy deposition (MOVPE)[272], template method[273], and hydrothermal method[274], etc. Therefore, it is suitable for growing ZnO nanowires with good field emission characteristics and is used to synthesize the nanowires in the present study.

It is well known that the structural properties and dopants may determine the electronic and photoluminescence properties of the material. The typical dopants that have been used to enhance the conductivities of ZnO are the group III elements (B, Al, In, Ga) and IV elements (Pb, Sn) of the periodic table. The Sn can serve as a doubly ionized donor when the incorporation of SnO_2 as a solute in ZnO and consequently provide high electron carrier concentration. It is, therefore, expected that the Sn doped ZnO (SZO) nanowires have higher electrical conductivity and better field emission properties compared to undoped ZnO nanowires.

In this work, the effects of varying the concentration of Sn as a dopant on the surface morphology, crystal structure, chemical composition, photoluminescence, and field emission characteristics of the undoped and SZO nanowires were investigated.

7.2 Experimental

To prepare the p-type Si (100) substrate for the synthesis of SZO nanowires, the substrate was cleaned by the standard Radio Corporation of America (RCA) cleaning method. After cleaning, the rf-sputtering (13.56 MHz) was adopted to deposit an ultra-thin Au catalyst film (~60 Å thick) under Ar sputtering gas (5.0 cm^3/min.) at 20 mTorr for ~10−30 sec. Our synthesis process was performed by a VLS fabrication process. The ball-milled (24 hr) and mixed powders of ZnO, SnO_2 and carbon (Alfa Aesar, 99.995%) were consisted of 0, 0.1 and 0.3 mole fractions of Sn. Then, the mixed powder was loaded into a quartz boat and placed in the center of a quartz tube. The cleaned p-Si(100) substrate was loaded in to the lower temperature region of the quartz boat. The quartz tube was laid in a horizontal furnace. The synthesis temperature of the VLS process of undoped ZnO and SZO nanowires were ~900 and ~800 ^oC, respectively. High purity Ar gas was used as carrier gas with the gas flow rate of 50−100 cm^3/min.

The crystal structure of the SZO nanowires was studied by X-ray diffraction (XRD, MAC Science, MXP18, Japan). The microstructures of those undoped and SZO nanowires were analyzed by field emission scanning electron microscopy (FE-SEM, Hitachi S-4700I, Japan) and high resolution transmission electron microscopy (HR-TEM, Philips tecani-20, U.S.A.). The chemical composition of the SZO nanowires was characterized by Analytical Transmission Electron Microscope (AEM/EDS, JEOL JEM-2010, Japan). The chemical bonding of the atoms of elements of the SZO nanowires was analyzed by X-ray photoelectron spectroscopy (XPS) and Auger electron microprobe (AES), respectively (VG Scientific ESCALAB 250, and 350, UK). A

photoluminescence analyzer (PL, Hitachi F-4500, Japan) with Xe lamp as an excitation source (325 nm) was used for optical emission studies at room temperature.

The field emission characteristics were measured by the Keithley 237 I-V analyzer which provided the sweeping electric field and monitored the emission current at a base pressure of 1×10^{-8} Torr at room temperature. The distance between the upper tungsten electrode probe and the SZO nanowires was 300 μm which adjusted by a precision screw-meter with an accuracy of ± 1μm and the area of this electrode was 0.028 cm^2.

7.3 Results and Discussion

The ZnO nanowires were grown in a horizontal quartz tube furnace. The p-Si(100) substrate and ZnO, SnO_2, and carbon ball mixed powders were loaded into the quartz tube. The p-Si(100) substrate that puts nearby the lower temperature zone of the furnace and makes sure loaded in the same position each experiment. During the synthesized process, high purity Ar gas as an auxiliary gas was induced into the fabrication system which flowing rate was 50−100 cm^3/min. The growth process continued at 800 to 900 ^oC for 12 to 20 min.

Figures 7.1(a), (b), and (c) indicate the XRD patterns of the ZnO nanowires with 0, 0.1and 0.3 mole fractions of Sn, respectively. The pure ZnO nanowires synthesized at 900^oC [Fig. 7.1(a)] are of hexagonal structure as reported in Joint Committee on Powder Diffraction Standards－International Centre for Diffraction Data (JCPDS-ICDD)[275] no. 80-0074. The reaction temperature for the formation of the SZO nanowires is not so high as that of the

undoped ZnO nanowires. It is suggested that SnO_2 react with carbon to form the Sn vapor according to the following chemical reaction:

$$SnO_{2(s)} + 2C_{(s)} \rightarrow Sn_{(g)} + 2CO_{(g)} \quad (7.1)$$

The generated Sn vapor would initiate a catalyst droplet-assisted growth in the early stage of VLS process. While we mixed SnO_2 and ZnO source powders with carbon, the synthesized temperature can be decreased to ~800°C.

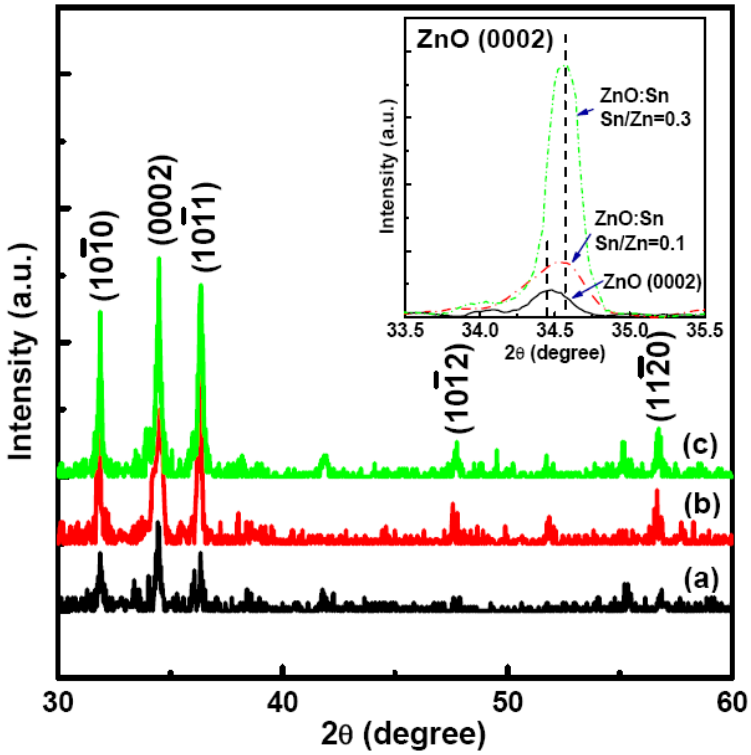

Figure 7.1 XRD patterns of the (a) ZnO, (b) 0.1, and (c) 0.3 SZO nanowires. The inset is (0002) peak shifted by Sn dopant.

The SZO nanowires synthesized at 800°C with 0.1 [Fig. 7.1(b)] and 0.3 [Fig. 7.1(c)] mole fraction of Sn have similar characteristic peaks as the pattern shown in the Fig. 7.1(a), but the 2θ of the (0002) peak has a little shift from 34.40° to 34.52°. The SZO nanowires are still of the hexagonal structure and possess shorter lattice parameter compared to the undoped ZnO nanowires. The lattice constants of the undoped ZnO nanowires are a = b = ~3.52 Å and c =

~5.21 Å, those of the 0.1 SZO nanowires are a = b = ~3.49 Å and c = ~5.19 Å, and those of the 0.3 SZO nanowires are a = b = ~3.43 Å and c = ~5.18 Å, which can be calculated according to the XRD patterns. If the addition of SnO_2 to ZnO forms a substitutional solid solution with the hexagonal structure, a possible reaction is:

$$SnO_{2(s)} \xrightarrow{ZnO} Sn_{Zn}^{\bullet\bullet} + 2O_O + V_{Zn}^{''} \qquad (7.2)$$

Where $Sn_{Zn}^{\bullet\bullet}$ means Sn substituted for Zn^{2+} in ZnO, O_O denotes O at oxygen site, and $V_{Zn}^{''}$ indicates a vacancy at a Zn^{2+} site in the lattice of the SZO nanowires. It is shown in Eqn. (7.2) that the Sn^{4+} atom is substituted for Zn^{2+} atom and the Zn vacancy forms. The shorter lattice constants in the SZO nanowires may be attributed to smaller ionic radii of Sn^{4+} ($r_{Sn}{}^{4+}$ = 0.069 nm, $r_{Zn}{}^{2+}$ = 0.074nm) and the formation of Zn-vacancy.

The tilted 45°−viewed FE-SEM images of undoped and SZO nanowires on p-Si(100) substrates are demonstrated in Fig. 7.2, indicating that the surface morphologies of the nanowires depend strongly on amount of the dopant, Sn. As shown in Fig. 7.2(a), the undoped ZnO nanowires have the smooth sidewalls, uniform diameter of ~50 nm and length of ~5 μm. Figures 7.2(b) and (c) show the geometrical appearances of the 0.1 and 0.3 SZO nanowires, respectively. Under the equal thickness of Au catalyst film (~60 Å), the geometrical appearances such as length and diameter of the ZnO nanowires should be similar due to the same thermal synthesized process and carrier gas flowing rate. But a very interesting aspect is the different morphologies for 0.1 and 0.3 SZO nanowires. These two nanowires have the rugged sidewalls, smaller diameters and longer lengths. The 0.1 SZO nanowires have a diameter of ~30 nm and length of ~10 μm, while the 0.3 SZO nanowires have a diameter

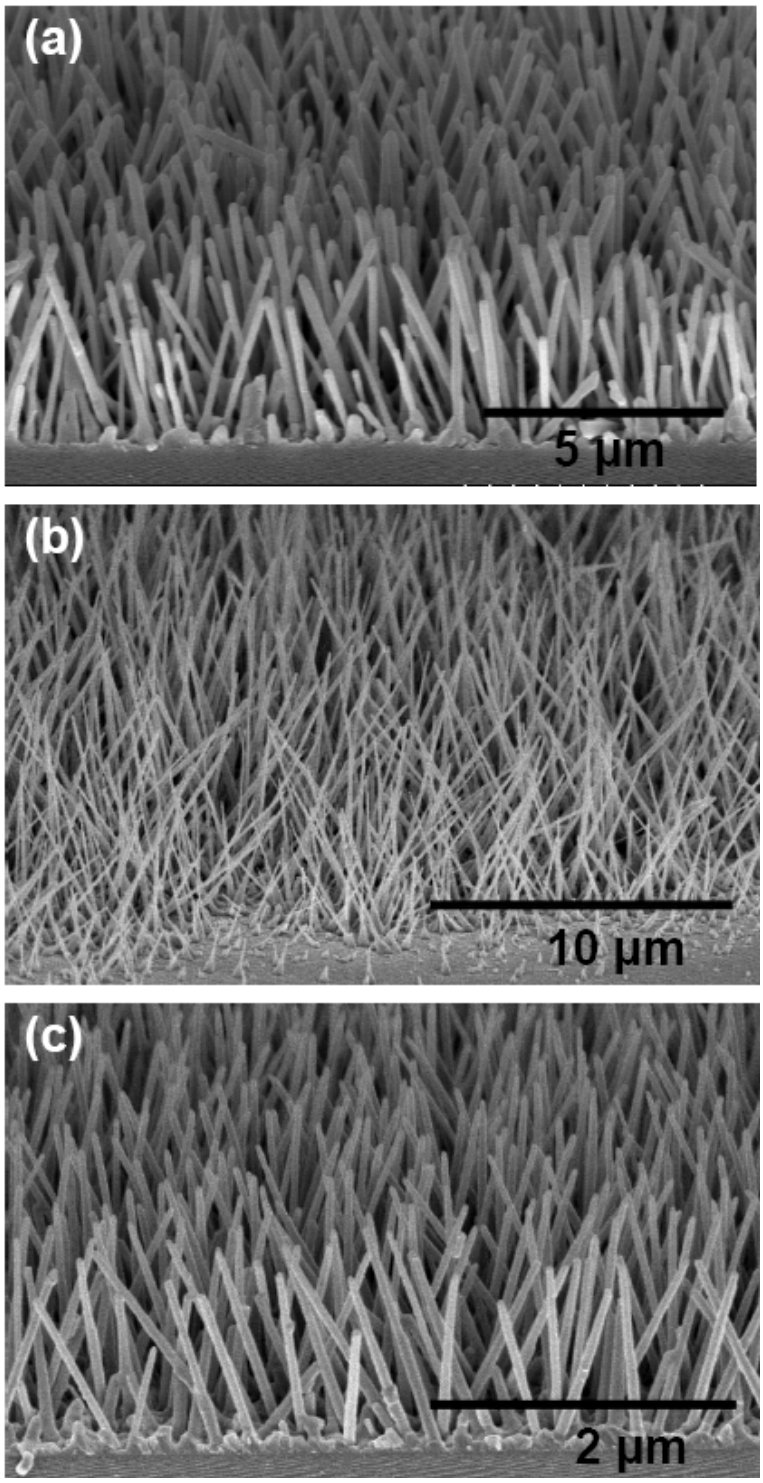

Figure 7.2 SEM images of the (a) ZnO, (b) 0.1, and (c) 0.3 SZO nanowires.

of ~80 nm and length of ~2 μm. The individual average volume of the undoped, 0.1, and 0.3 SZO nanowires are of the same order and comparable. The values

are ~9.817×10^{-3}, ~7.068×10^{-3}, and ~10.053×10^{-3} μm^3, respectively. According to the alloy phase diagram of Au and Sn, at the temperature of ~282 ^oC, Au and Sn form an eutectic Au-Sn alloy (20 wt% Sn and 80 wt% Au).[276] Therefore, the 0.1 SZO nanowires have the smaller diameter and longer length because of the low partial pressure of Sn in vapor phase in the upstream that leads to the deposition of Sn as small droplets that alloying with Au on the substrate, thus initiating the growth of longer nanowires in the presence of sufficient Zn vapor in the VLS process. On the contrary, the 0.3 SZO nanowires have larger diameter and shorter length due to the presence of abundant Sn vapor that leads to the formation of larger Au−Sn catalyst droplets under an lower Zn vapor pressure. The Sn−assisted growth mechanism of undoped and SZO nanowires is schematically shown in Fig. 7.3. The Sn in the alloy droplets can diffuse into ZnO nanowires through the thermal process. The content of Sn in the SZO nanowires can be measured by EDS spectra as demonstrated in a later section. This indicates that the fraction of Sn to Zn can influence the morphologies of the SZO nanowires.

The HR-TEM images of the SZO nanowires shown in Fig. 7.4 depict the effect of doping on the slip system. The clear lattice fringes of (0002) planes of 0.1 SZO nanowires are indicated in Fig. 7.4(a) and there exists an included angle of ~70^o between the [0002] direction and the growth direction. The distance between each lattice fringe is 3.49 Å that matches the lattice constants (a = b = ~3.49 Å and c = ~5.19 Å) obtained from the XRD analysis (Fig. 7.1). The 0.3 SZO has ~3.43 Å between two (0002) planes [Fig. 7.4(b)], which is also consistent with XRD results (a = b = ~3.43 Å and c = ~5.19 Å.) with an included angle of ~88^o between the [0002] direction and the growth direction. The accurate Sn contents of 0.1 and 0.3 Sn doped SZO nanowires are ~0.24

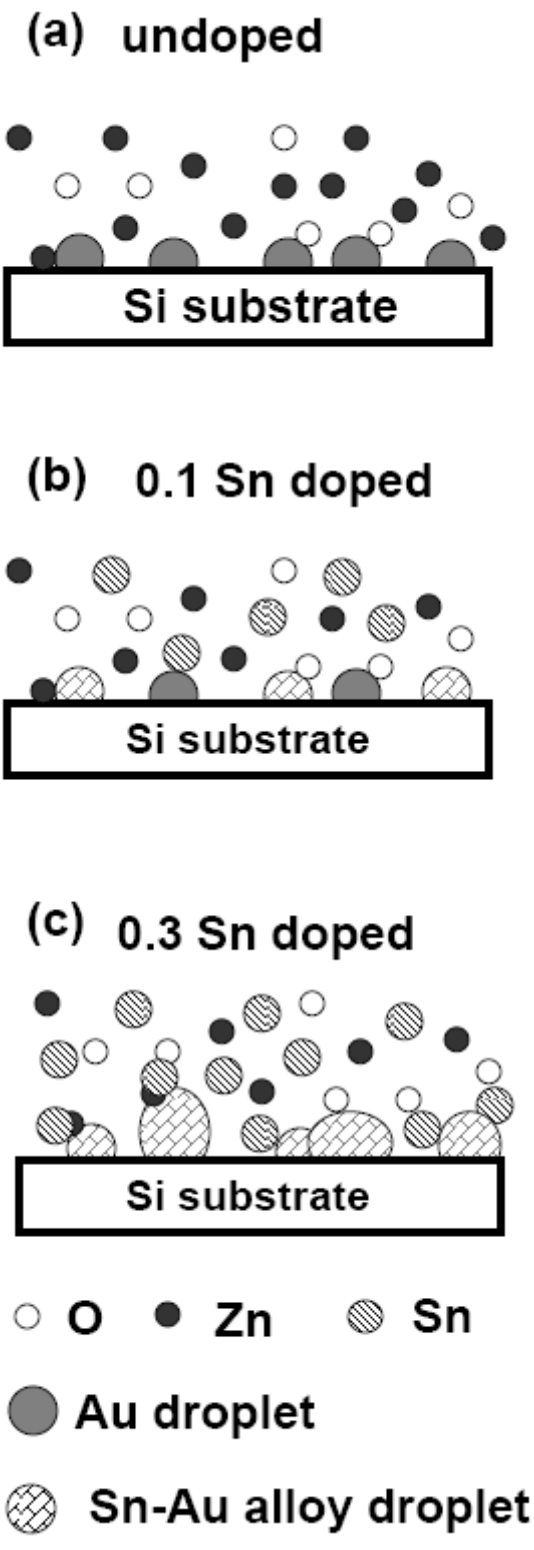

Figure 7.3 VLS growth process mechanism for, (a) undoped, (b) 0.1 and (c) 0.3 SZO nanowires.

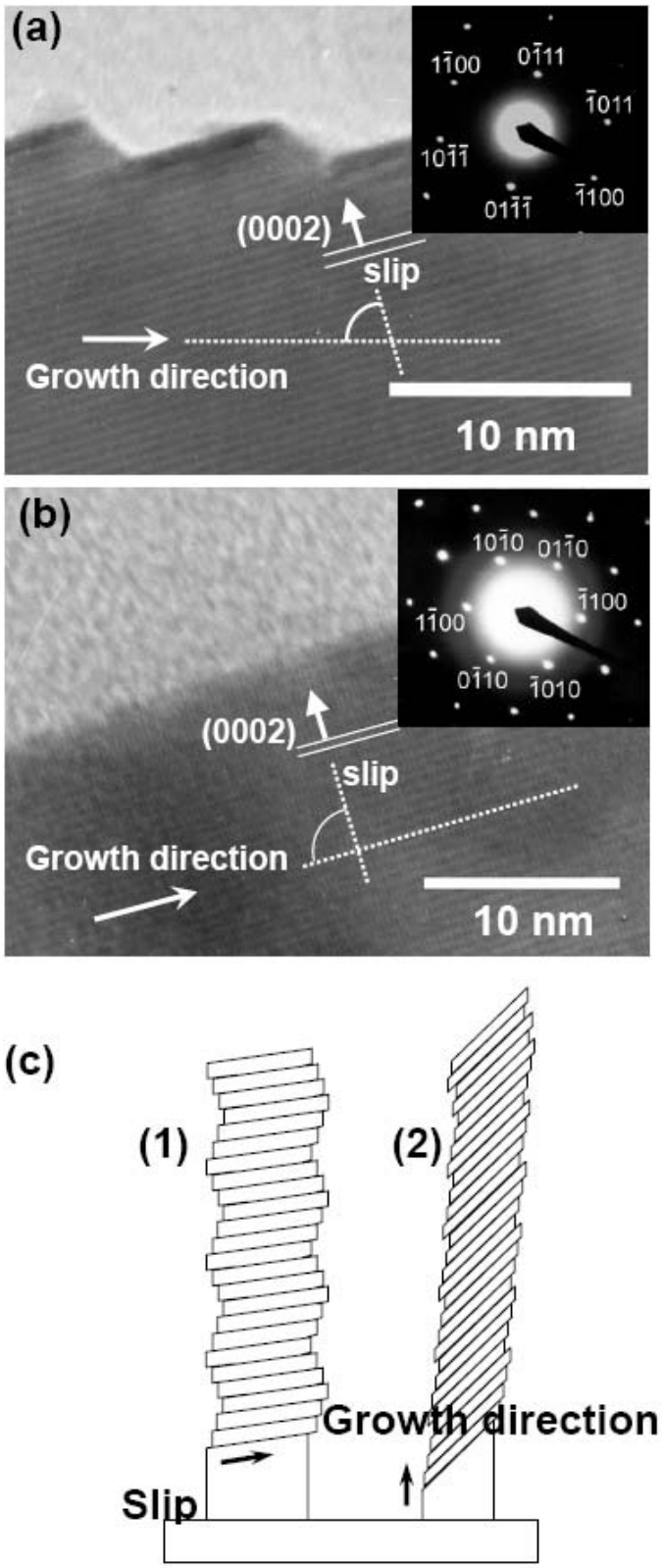

Figure 7.4 (a) HR-TEM images of the 0.1 SZO nanowires. The (0002) lattice fringe is tilted by about 70^{o} with growth direction. The inset is SAED pattern. (b) HR-TEM images of the 0.3 SZO nanowires. The (0002) lattice fringe is tilted by about 88^{o} with the growth direction. The inset is SAED pattern. (c) The slip structure with the different molar fractions of Sn in SZO nanowires.

and ~0.60 at.%, respectively on the basis of the AEM-EDS and XPS analysis results in the later section. Such an increase in the included angle with an increase in Sn concentration (Fig. 7.4) may be attributed to larger compressive stresses generated in higher Sn concentration nanowires, arising from the difference in thermal expansion coefficients as a result of smaller ionic radii of Sn in comparison with that of Zn ($r_{Zn^{2+}}$ = 0.074 nm and $r_{Sn^{4+}}$ = 0.069 nm) and higher amount of Zn vacancies existed in higher Sn doped nanowires based on Eqn. (7.2). That is, the enhanced compressive stress and increased amount of Zn vacancies in higher Sn doped nanowires would consequently lead to an larger included angle between the [0002] direction and the growth direction. Therefore, the variation of mole fraction of the dopant Sn would influence the internal stress resulting in the different slip structures of the SZO nanowires [Fig. 7.4(c)]. The SAED patterns shown in the insets of Figs. 7.4(a) and (b) indicate the $[01\bar{1}0]$ direction and hexagonal structure of the SZO nanowires, respectively.

The AEM-EDS spectra of the SZO nanowires are shown in Fig. 7.5. Figure 7.5(a) is a typical spectrum of SZO nanowires and the corresponding chemical compositions have also been marked (the Cu peaks come from Cu TEM grid). It reveals that zinc (Zn), oxygen (O) and tin (Sn) are the constituent parts of the SZO nanowires, and the compositions are uniform along the growth direction. The EDS measurements show that the dominant composition is $Zn_{0.977}Sn_{0.024}O$ for the 0.1 SZO and $Zn_{0.941}Sn_{0.060}O$ for the 0.3 SZO nanowires. The measured Sn at.% may be due to the diffusion of excess Sn from Sn saturated Au−Sn alloy droplet. At beginning of the VLS fabrication process, Sn is expected to form a eutectic alloy with Au. Upon extending the fabrication

time, Sn partial pressure gets saturated. This leads to precipitation of Sn from the Au-Sn alloy and its diffusion into the ZnO nanowires. That means, most of the Sn remain in front of the metal tip of the SZO nanowires and adapt to burning away by longer synthesized time under flowing carrier Ar gas. Therefore, Sn doping concentration of the SZO nanowires depends on the SnO_2 mole fraction presented in the ball milled and mixed powders.

The XPS spectra of 0.3 Sn doped nanowires are shown in Fig. 7.6, indicating that the Sn^{4+} has substituted for Zn^{2+} and hence Zn-vacancy has formed. In Fig. 7.6(a), $Zn_{2p3/2}$ and $Zn_{2p1/2}$ peaks are located at 1026.8 and 1045.1 eV, respectively. And in Fig. 7.6(b), the O_{1s} is located at 531.2 eV. Based on the binding energy spectra, the $Zn_{2p3/2}$ and $Zn_{2p1/2}$ peaks that appear respectively at 1026.8 and 1045.1 eV and coincide with the previous XPS findings for ZnO[277]. The O_{1s} peak at 531.2 eV is attributed to oxidized ions in ZnO nanowires. Furthermore, the $Sn_{3d5/2}$ and $Sn_{3d3/2}$ peaks shown in Fig. 7.6(c) are located at 487.1 and 495.1 eV, respectively, which can be attributed to Sn ions in the SZO nanowires. The mole fraction of Zn/Sn/O is ~0.934/0.067/1.000 calculated from XPS data, which reasonably agrees with AEM-EDS result for 0.3 Sn doped nanowires. The chemical state energies of the detected Sn and O in the SZO nanowires exhibit Sn−O bonds formation, that is, Sn atom can diffuse into the ZnO nanowires and the Zn^{2+} is substituted by Sn^{4+} leading to an increase in concentration of electrons and will consequently lead to better field emission characteristics of the SZO nanowires, which is described in a subsequent section.

The high resolution AES chemical composition spectra of 0.3 Sn doped SZO nanowires can further decide the bonding between the atoms of SZO nanowires. Figure 7.7(a) is an AES spectrum of the SZO nanowires scanned in

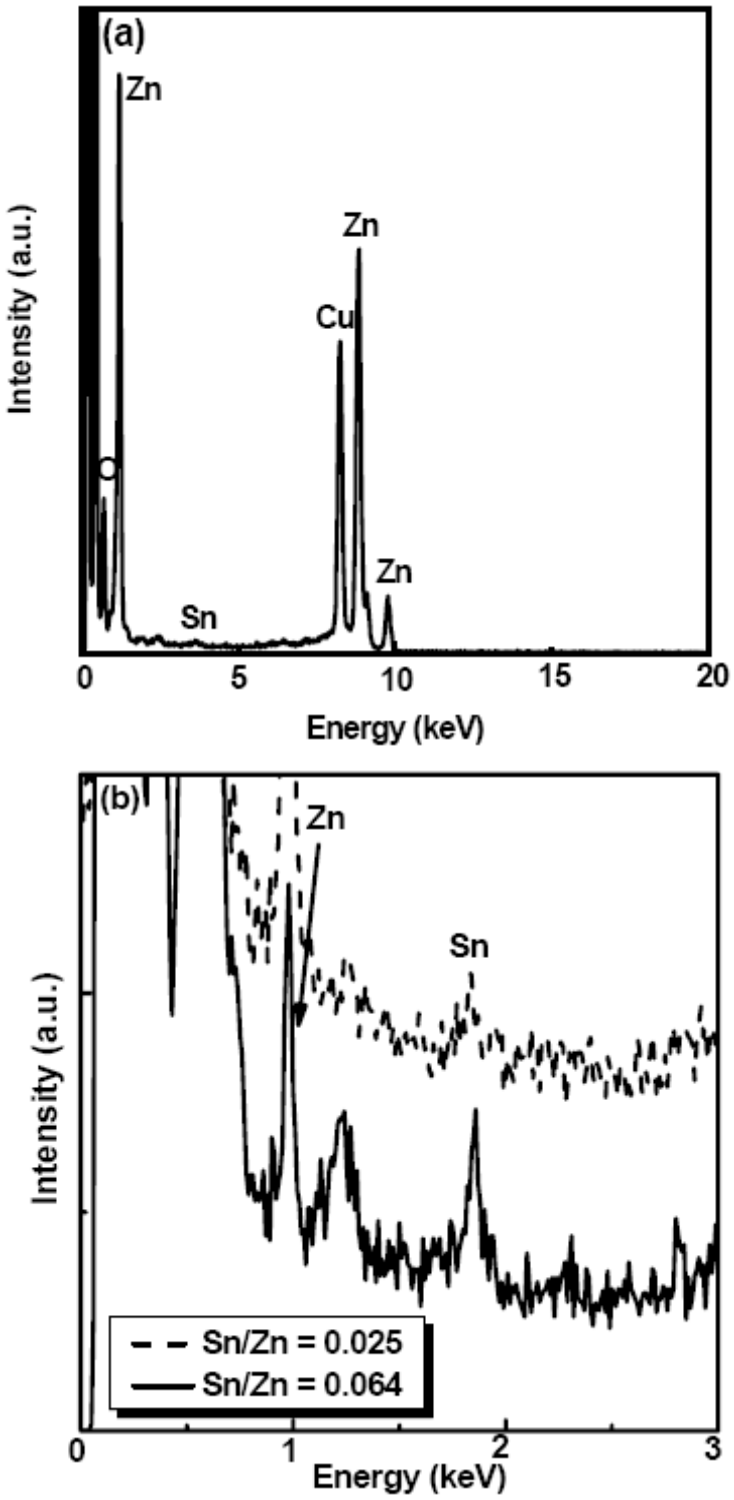

Figure 7.5 (a) EDS spectrum of the SZO nanowires and (b) enlarged EDS spectra of the SZO nanowires.

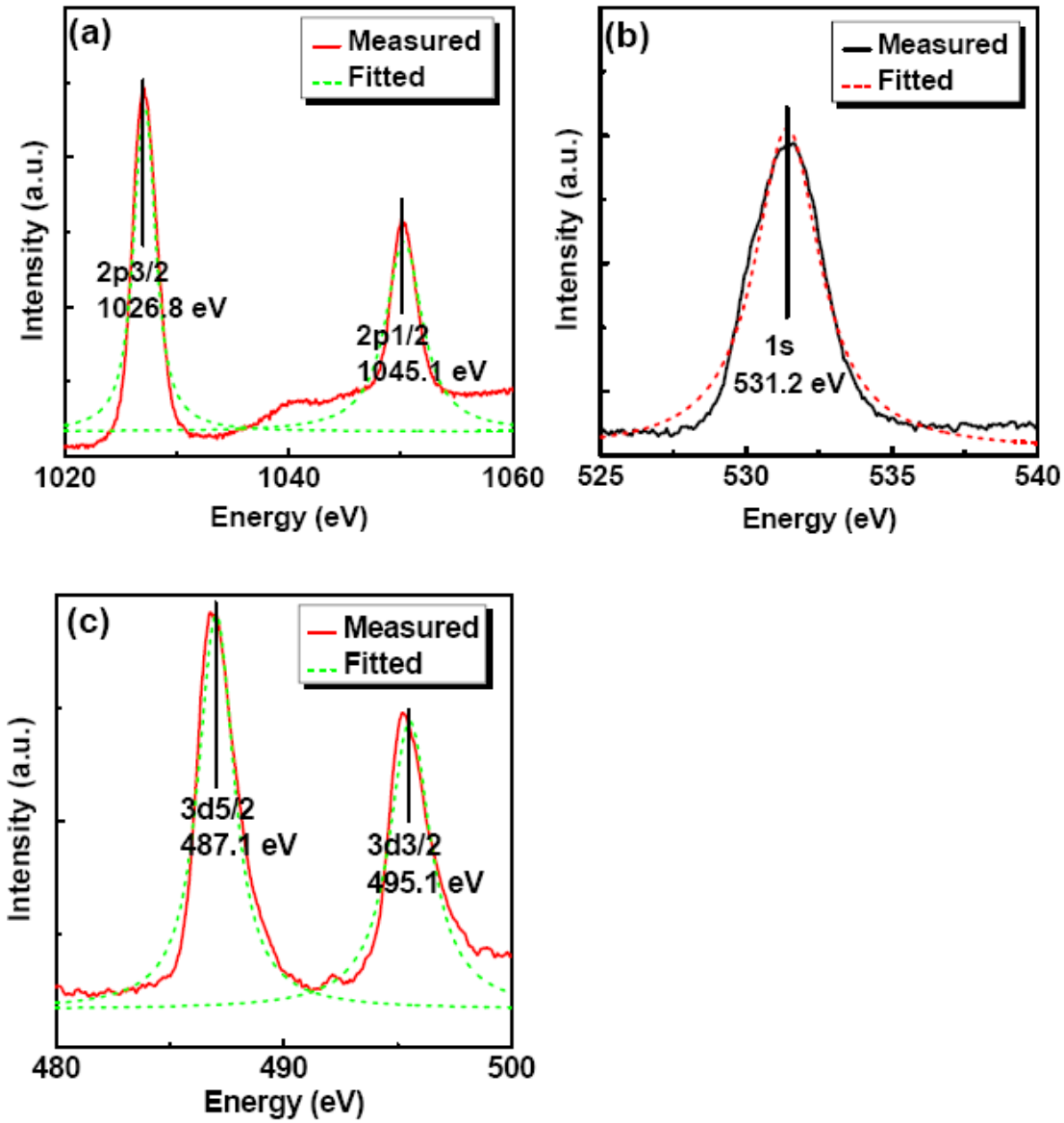

Figure 7.6 XPS spectra of the 0.3 Sn doped SZO nanowires, (a) Zn spectrum, (b) O spectrum, and (c) Sn spectrum.

the full scanning range (300 to 1200 eV). After differential calculation analysis, some obvious peaks indicate the Sn, Zn, and O are located at 400-440 eV, 990-1020 eV, and 480-510 eV, respectively[21]. The detailed high resolution binding energy spectra of individual element are shown in Figs. 7.7(b), (c), and (d). The AES spectrum of Zn [Fig. 7.7(b)] indicates clear peaks at 986.4, 988.6 and 1012.7 eV corresponding to the LMM Auger electron emissions from the

Zn−O bonds. The vibration curve between 991.6 and 995.2 eV is resulted from Zn−Zn bonds. Figure 7.7(c) shows the MNN emissions of Sn−O bonds, which are located at 421.5, 430.2 and 432.4 eV while the 425.4 eV emission results from Sn−Sn bonds. Lastly, the oxygen KLL emissions of 490.3 eV and 509.4 eV are indicated in Fig. 7.7(d). On the basis of AES result, we may presume that the Sn substitutes Zn and binds with O in the SZO nanowires, which is in agreement with the result of XPS analysis.

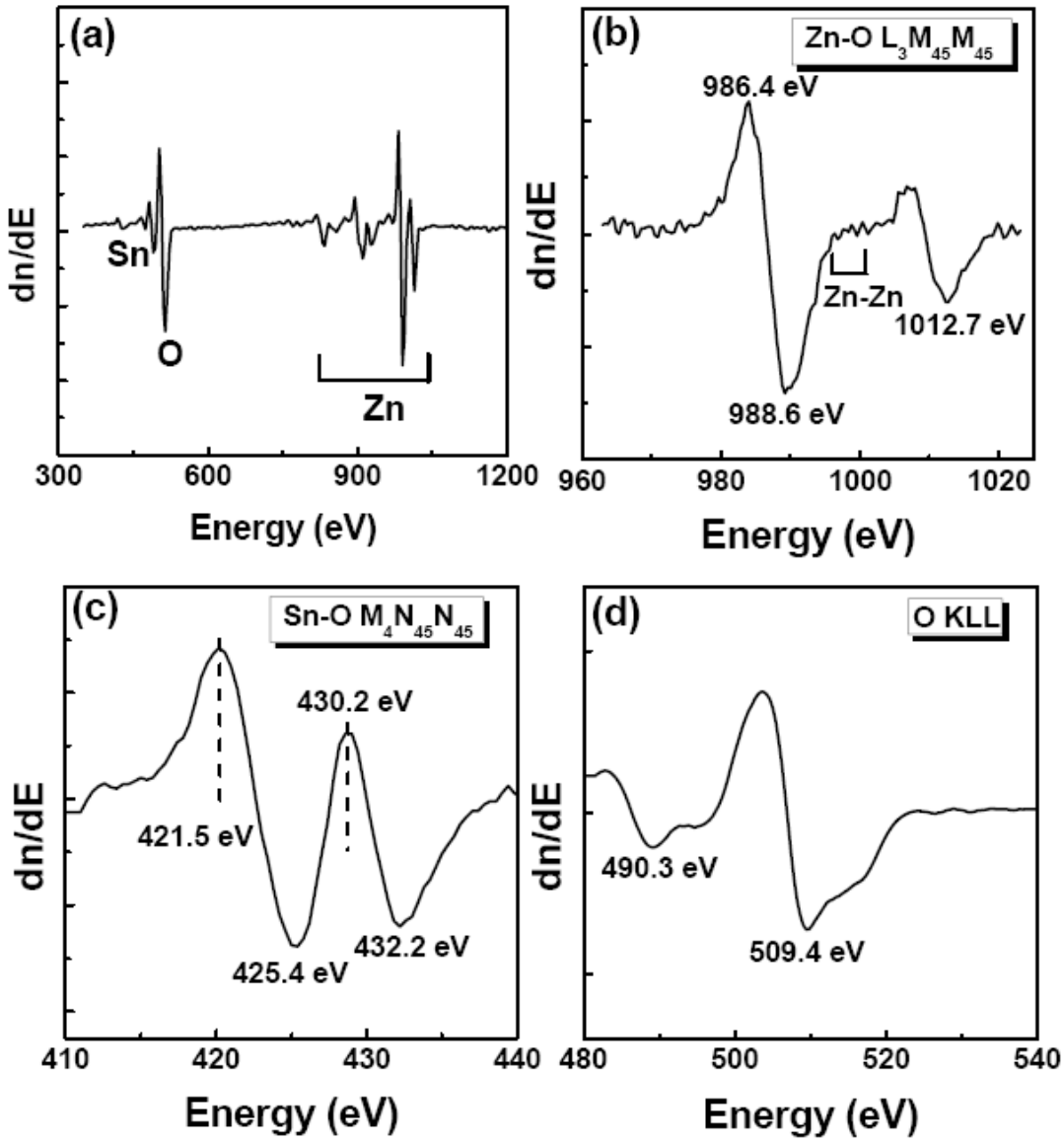

Figure 7.7 AES differential spectra of the 0.3 Sn doped SZO nanowires, (a) full scale scanning results. (b) Zn spectrum, (c) O spectrum, and (d) Sn spectrum.

Figure 7.8(a) shows the room temperature (298 K) photoluminescence (PL) spectra of undoped ZnO and SZO nanowires. A strong UV emission at 380 nm and a green light emission at 520 nm are observed in the PL spectrum of the undoped ZnO nanowires. The UV emission is due to the direct band gap of ZnO, and the green light emission is corresponding to the oxygen vacancies in the ZnO nanowires. On the other hand, it illustrates that the SZO nanowires exhibit four photoluminescence bands centered at 380, 396, 461 and 502 nm. Corresponding to the band gap value of the SZO nanowires shown in Fig. 7.8(b), those two emission peaks at 380 nm(E_λ = 3.26 eV) and 396 nm(E_λ = 3.13 eV) could be attributed to (1) the recombination of electrons in valence band with holes in conduction band, and (2) the recombination of electrons in deep traps with holes in conduction band, respectively. These processes are shown in Fig. 7.8(c). It is suggested that the first peak of 380 nm correspond to the band gap of ZnO, and the second peak of 396 nm may be due to the response for the Sn atom that performs the role of a doubly ionized donor and introduces deep states in the energy band gap [see Fig. 7.8(c)]. As a result, the peak intensity of 396 nm caused by 0.3 SZO nanowires is higher than that of the 0.1 SZO nanowires. There are other two broad photoluminescence emissions, 461(E_λ = 2.68 eV) and 502(E_λ = 2.47 eV) nm in the spectra of the SZO nanowires, which may be associated with a complex luminescent centers such as $(V'_{Zn} - Sn^{\bullet\bullet}_{Zn})^{\bullet}$ or Zn_i[278-279]. Other minor unknown peaks in Fig. 7.8 possibly result from the phonons or photons emission process associated with the thermal atomic vibration in the nanowires.

The field emission characteristics of the undoped ZnO and SZO nanowires are shown in Fig. 7.9(a). At the current density of 0.5 mA/cm^2, the turn on

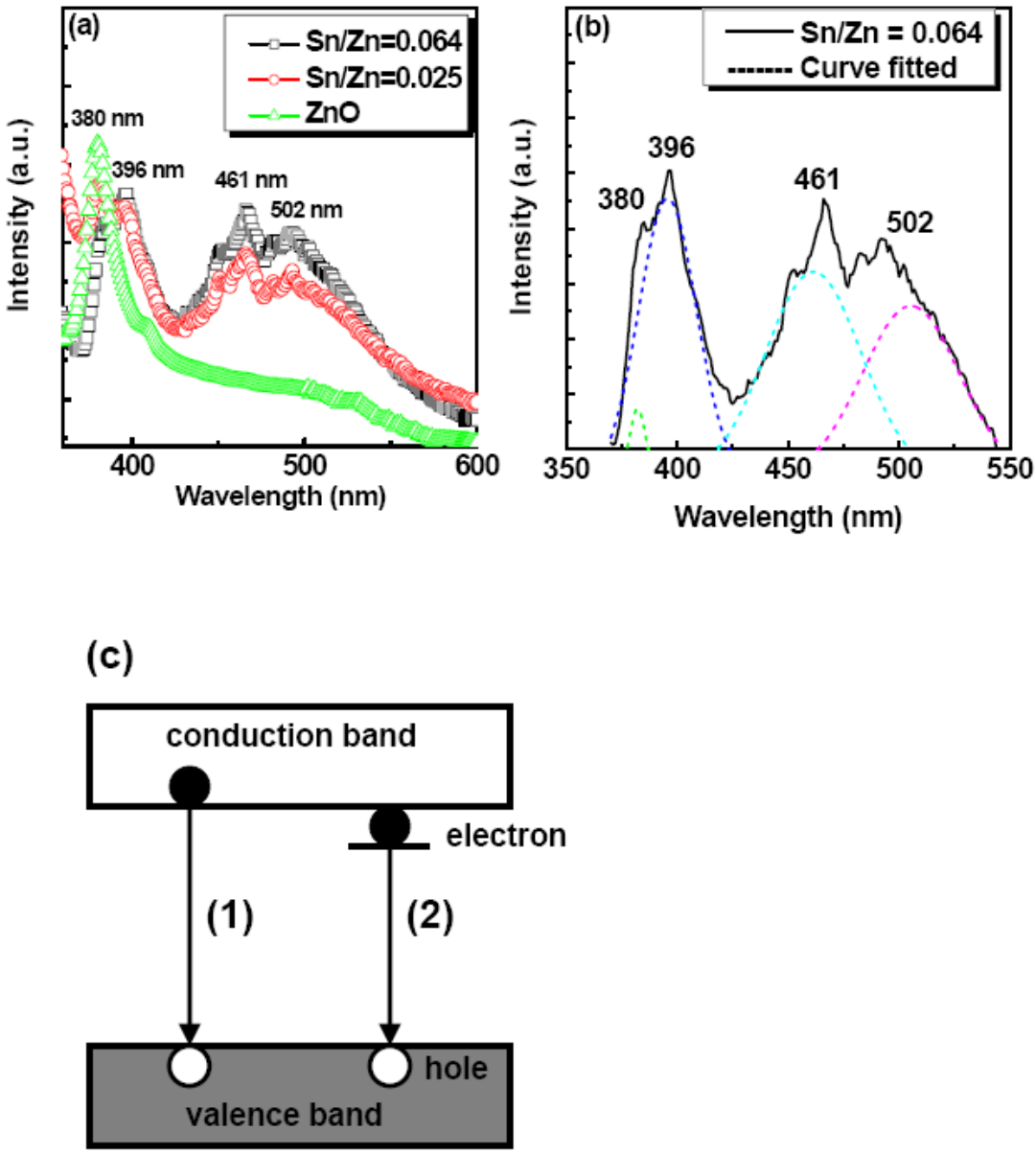

Figure 7.8 (a) PL emission spectra of the updoped and SZO nanowires. (b) PL emission curve fitted analysis for 0.3 SZO nanowires. (c) proposed energy band structure of the undoped and the SZO nanowires.

electric fields of undoped, 0.1 and 0.3 SZO nanowires are 0.83, 0.07 and 0.05 V/μm, respectively. While the electric field is remained at 0.05 V/μm, the electron number densities from the field emission mechanism of the ZnO nanowires are 2.97×10^{15} for 0.3 SZO, 9.93×10^{14} for 0.1 SZO, and 3.77×10^{14} for undoped ZnO nanowires. The released electrons may be increased due to

the increase in electric field, and Sn dopant as proposed in Eqn. (7.1). The lower turn on electric field and higher electron number density again provide evidence of the substitution of Zn by Sn in the SZO nanowires. The SZO nanowires exhibit the better field emission properties than that of the undoped ZnO nanowires. After the I-V measurement, the Fowler–Nordheim (F-N) relation ($\ln(I^2/E)$ is plotted as a function of *1/E*) is applied in order to realize the properties of those emitters The F-N plots [indicated in Figs. 7.9(b), (c) and (d)] of those nanowires indicate that the field emission properties of those nanowires follow the F-N equation[280]:

$$J = \frac{A\beta^2 E^2}{\phi}\exp\left(\frac{-B\phi^{3/2}}{\beta E}\right) \tag{7.3}$$

where J is the current density, E the applied field, ϕ the work function of the emitter, β the field enhancement factor, $A = 1.56\times10^{-10}$ (AV^{-2} eV) and $B = 6.83\times10^{3}$ ($VeV^{-3/2}$ Vμm^{-1}). Therefore, the field enhancement factor and work function can be obtained respectively from the slope and the intercept of the $F-N$ plot. The work functions Φ of undoped, 0.1, and 0.3 SZO nanowires are 7.26, 7.16, and 6.92 eV, respectively, while field enhancement factor, β, of those nanowires are 2.07x10^4, 4.45x10^5 and 6.67x10^5, respectively. The better experimental results are obtained for 0.3 SZO nanowires : β = 6.67x10^5 and Φ = 6.92 eV. The field enhancement factors increase and the work function decreases due to the addition of Sn. The larger field enhancement factor is attributed to the smaller diameter of the SZO nanowires. Moreover, it can be concluded from the result that the Sn dopant acts as the donor, which increases the carrier concentration and reduces the work function of the SZO nanowires.

To investigate the difference of electronic characteristic between undoped and SZO nanowires, the stability of the field emission current-voltage

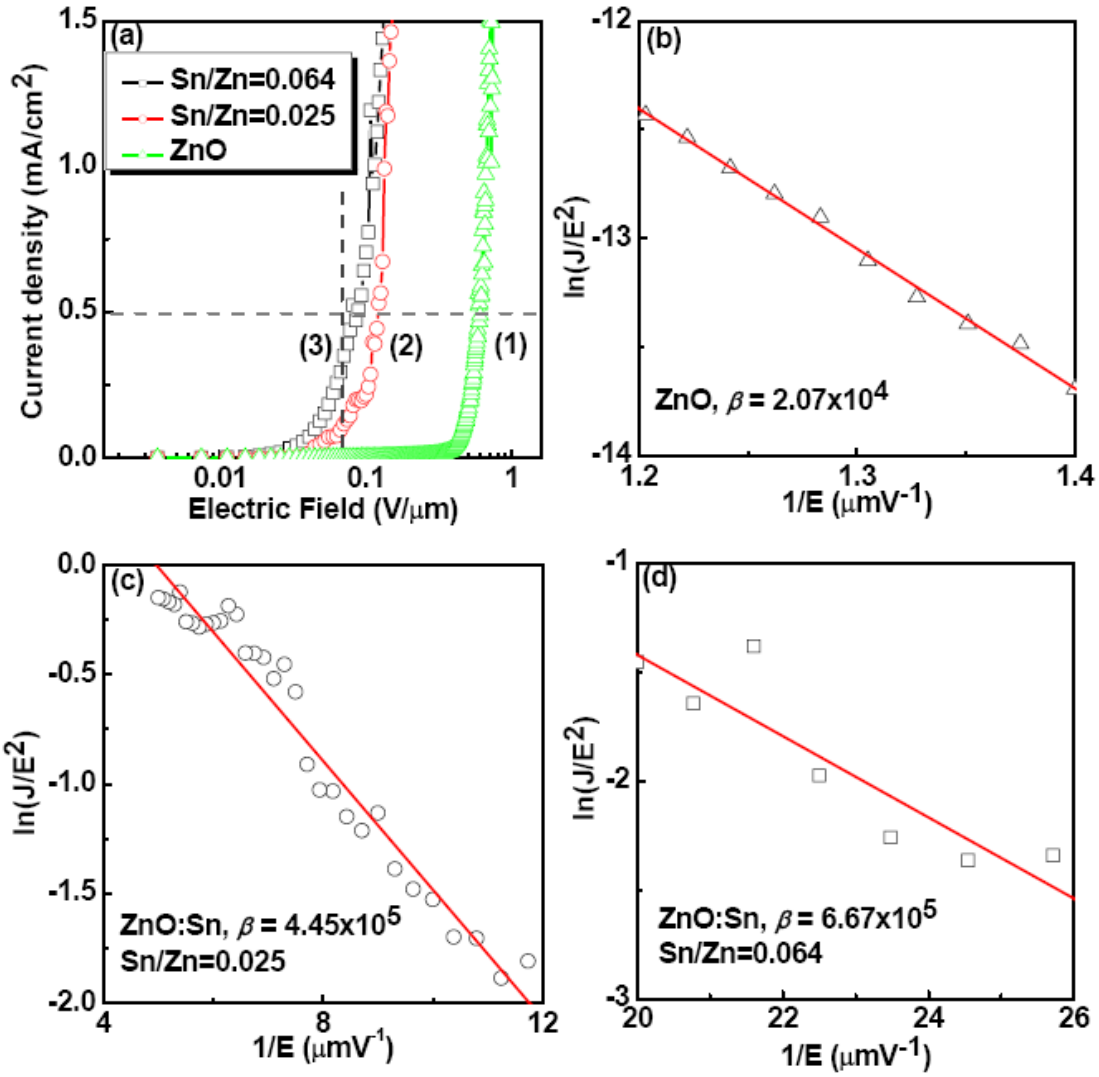

Figure 7.9 (a) Field emission characteristics of the ZnO, (b) F-N plots of undoped ZnO, (c) F-N plots of 0.1 Sn doped, and (d) F-N plots of 0.3 Sn doped ZnO nanowires.

characteristic is compared, as shown in Fig. 10. The saturation behavior has been observed on individual unoped, 0.1 and 0.3 doped ZnO nanowires. The saturation of the field emission current has occurred in those nanowires, that is, each ZnO nanowire has its highest resistance under the turn on electric field[281-282]. In this case, the voltage drop (*IR*) across such resistor would lead to decrease in the effective applied voltage, and therefore to cause a flattening of the characteristics. The resistance in series with the ZnO nanowires can be

estimated by using

$$I = a(V - IR)^2 \exp[-b/(V - IR)] \quad (7.4)$$

where I and V are field emission current and applied voltage, respectively, a, b are constant, and R is resistance in series with the ZnO nanowires. Firstly, assuming R = 0, a and b can be evaluated by Eqn.(7.4) fitting to the low emission current part of the measured data. The resistances corresponding to undoped, 0.1 and 0.3 SZO nanowires are estimated to be 85.43, 24.53, and 8.53 kΩ, respectively, as shown in Fig. 7.10. This decrease in resistance is proportional to the increase in Sn dopant concentration. The lower resistance of SZO nanowires is also attributed to that Sn−enhanced the electron density and consequent increase of the conductivity of the ZnO nanowires.

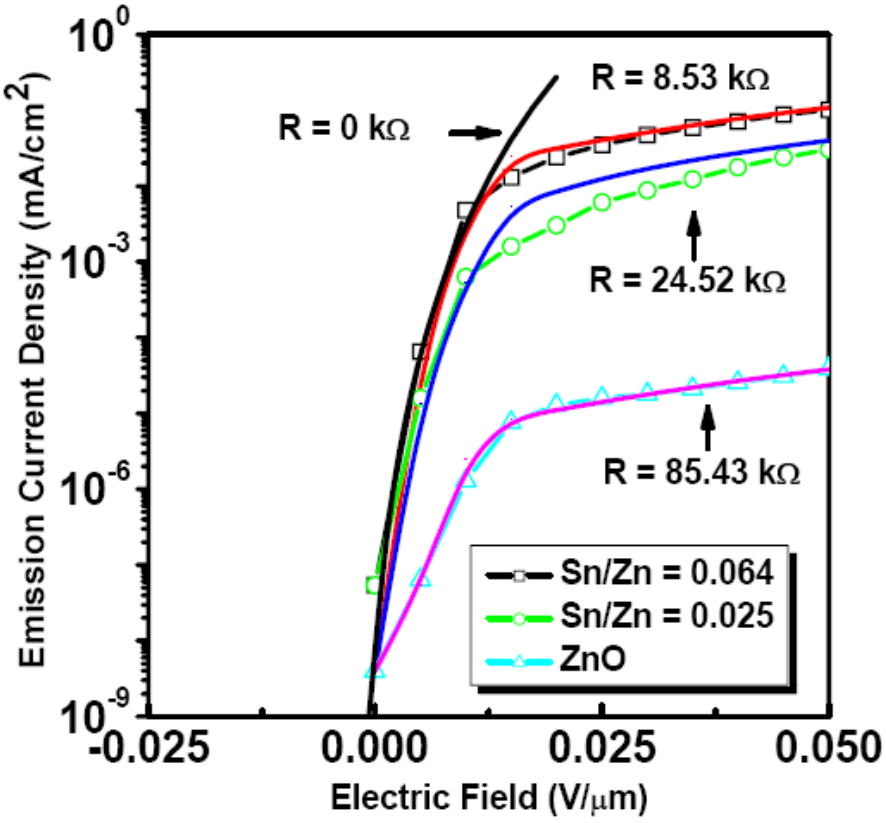

Figure 7.10 Emission current density vs. electric field of the undoped, 0.1, and 0.3 SZO nanowires.

7.4 Summary

In summary, the single crystalline SZO nanowires are fabricated at 800 ^{o}C under the conditions of a vapor-liquid-solid (VLS) growth process. The morphologies of SZO nanowires is quite different from the undoped ZnO nanowires due to the occupancy of Sn atom at the Zn site. This Sn addition also affects the ultra-violet (UV) emission of SZO nanowires. Furthermore, the 0.3 SZO nanowires exhibit good field emission characteristic of 0.05 V/μm as the turn−on electric field and 0.5 mA/cm^2 as the current density. The lower work function of the SZO nanowires is due to the higher carrier concentration and the smaller diameters that result in the higher field enhancement factor. Therefore, the SZO nanowires could be used for fabricating optoelectronic and field emission devices.